buildings

MDPI

Article

Experimental and Numerical Investigation on the Bearing Capacity of Axially Compressive Concrete-Filled Steel Tubular Columns with Local Corrosion

Wei Fang [1,2], Mengcheng Chen [1,2,*], Qingqing Wen [1,2], Hong Huang [1,2], Kaicheng Xu [1,2] and Rui Zhang [2]

[1] State Key Laboratory of Performance Monitoring and Protecting of Rail Transit Infrastructures, Nanchang 330013, China
[2] School of Civil Engineering and Architecture, East China Jiaotong University, Nanchang 330013, China
* Correspondence: mcchen@ecjtu.jx.cn

Abstract: This study aims to examine the effects of local corrosion on the axial compression performance of concrete-filled steel tubular (CFST) members. Nineteen CFST short columns with local corrosion were designed and fabricated to undergo axial compression mechanical property tests, with the radial corrosion depth of the local corrosion area as the key test parameter. The failure mechanism and mechanical property change laws of CFST axial compression short columns with circumferential full corrosion at the ends and middle were studied. Combined with finite element modeling, the influence laws of the three-dimensional geometrical characteristics of the local corrosion zone, i.e., the axial length, the annular width and the radial depth, on the structural bearing performance were thoroughly explored and discussed. The results revealed that the main reason for the reduction in load-carrying capacity of circular CFST axial columns due to local corrosion is attributed to the reduction of the effective cross-sectional area of the steel tube in the corrosion area. When local corrosion occurs at different axial positions, the variation range of the bearing capacity of CFST columns is within 10%. Regarding the impact of the three dimensions of local corrosion on the axial load-carrying capacity of CFST, the radial corrosion depth was identified as the most influential factor, followed by the annular corrosion width, and finally by the axial corrosion length. When the axial corrosion length exceeds 20% of the specimen length, its further influence on the load-carrying capacity is considered limited. Finally, a practical calculation formula for the bearing capacity of locally corroded CFST columns is proposed. The predicted results of this formula fit well with the test results and can quickly estimate the remaining bearing capacity of the structure by measuring the geometric parameters of the local corrosion area, providing a reference for the assessment and maintenance of CFST structures.

Keywords: concrete-filled steel tubular; local corrosion; axial compression test; finite element analysis; bearing capacity calculation

Citation: Fang, W.; Chen, M.; Wen, Q.; Huang, H.; Xu, K.; Zhang, R. Experimental and Numerical Investigation on the Bearing Capacity of Axially Compressive Concrete-Filled Steel Tubular Columns with Local Corrosion. *Buildings* **2024**, *14*, 3628. https://doi.org/10.3390/buildings14113628

Academic Editor: Vipul Patel

Received: 18 October 2024
Revised: 8 November 2024
Accepted: 12 November 2024
Published: 14 November 2024

1. Introduction

Concrete-filled steel tubular (CFST) structures, which have superior mechanical properties such as light self-weight, high load-bearing capacity, good seismic performance, and overall stability compared to traditional reinforced concrete structures and steel structures, are widely used in modern bridge engineering. However, the service environment of the structures is complex, such as environmental corrosion, cyclic loads, and the coupling of the two, which cause and exacerbate corrosion damage on the surface of CFSTs. Corrosion not only degrades material properties and weakens the steel tube's confinement effect to the core concrete, but also affects the durability and operational performance of the CFST structures [1,2]. In bridge and civil architecture structures, the CFST members are usually used as columns or bars to bear compression [3]. Therefore, the study of the evolution law

of axial compressive mechanical properties of corroded CFST columns is of great theoretical and practical significance for assessing the safety and reliability of such structures.

At present, scholars have carried out research on the working performance of CFSTs after corrosion. Han and Hou et al. [4–7] carried out experimental research on the stress performance of CFST members under the coupling action of chloride ion corrosion with long-term loading and used finite element numerical and theoretical analyses to obtain the calculation method of the residual bearing capacity of the members considering chloride ion corrosion. Hua et al. [8] developed a finite element model for the axial tensile mechanical properties of CFSTs under chloride ion erosion and long-term loading and verified it with experimental data. Wang et al. [9,10] pointed out in their research that the combined action of corrosion and load will exacerbate the degradation of the mechanical properties of CFST members. Xu et al. [11] developed a finite element model based on stochastic theory and carried out a reliability analysis of the axial bearing capacity of CFST columns under the coupling effect of corrosion and loading. Gao et al. [12] conducted an experimental study on the performance degradation of circular thin-walled CFST columns in high-latitude offshore areas and proposed a theoretical formula for calculating the load-bearing capacity of circular thin-walled CFST columns under freeze–thaw cycles and corrosive environments. Zhang et al. [13] carried out accelerated corrosion tests on circular CFST columns with different wall thicknesses to study the influence of corrosion on their axial compressive load-bearing capacity. Zhang et al. [14] experimentally designed 40 square CFST columns to study their axial performance degradation law under the freeze–thaw cycle and corrosion environment and proposed a simplified calculation method for the ultimate load strength of CFST columns after damage. Chen et al. conducted systematic research on the mechanical properties of concrete-filled steel tube members under simulated acid rain corrosion [15–17]. Their research scope covers multiple key aspects such as the cooperative working mechanism, static performance, and seismic performance of corroded CFST members, accumulating abundant and valuable information in this field. Although the above research results are fruitful, most existing studies mainly focus on the impact of full surface corrosion on the structural performance of CFST structures. In the complex environment of actual engineering projects, full surface corrosion is relatively uncommon. In actual situations, due to various factors such as damage to the protective layer, local corrosion is more likely to occur [18].

Compared to full surface corrosion, the impact of local corrosion on structural performance presents higher complexity. It not only involves changes in material properties and stress distribution within the corroded zone itself but also may trigger changes in the overall stress pattern of the structure, such as causing local stress concentration and changes in sectional geometric characteristics, thereby affecting the overall stability and bearing capacity of the structure [19,20]. Guo et al. [21,22] fabricated artificial notches on the surface of CFST columns to simulate local groove corrosion defects and studied the axial compressive performance of CFST short columns with groove corrosion defects, and proposed the corresponding bearing capacity calculation formula. Li [23,24] and Zhao [25] focused on the study of the influence of random pitting corrosion on the axial compressive performance of CFST columns. Li et al. [26,27] further proposed the calculation method of the bearing capacity of CFST columns considering random pitting corrosion. These studies have achieved certain results in revealing the influence law of pitting corrosion, a form of local corrosion, on the structural performance, especially emphasizing the significant influence on CFST structural performance when pitting corrosion gradually expands during the corrosion development process. However, such studies have not deeply explored the influence differences of the geometric size changes of different local corrosion areas on the structural performance. In view of this, the authors [28] simulated the surface corrosion of long CFST columns and analyzed the mechanical property changes under various corrosion patterns, further enriching the content of local corrosion research. However, overall, most of the previous studies explored the influence of local corrosion on the mechanical properties of CFST structures by taking the overall corrosion rate as a variable, which has certain limitations.

Based on the previous research process, we have realized that, under the same corrosion rate, the changes in the three-dimensional size (axial length, annular width, and radial depth) of the local corrosion area have a significant impact on the mechanical properties of CFST structures. In view of this, we cannot ignore this difference. To study this question in depth, this paper selects the radial corrosion depth as the test design parameter and designs 19 circular CFST short columns with local corrosion to conduct axial compression tests. The aim is to observe the influence of local corrosion on the force characteristics and damage morphology evolution of the members during the entire axial compression process. On the basis of experimental verification, ABAQUS 6.14.2 software is used to focus on analyzing the influence law of the three-dimensional size of the local corrosion area on the mechanical properties of CFST columns. By combining the experimental results with the finite element simulation results, this study proposes a practical calculation formula for the bearing capacity of CFST columns considering the influence of local corrosion.

2. Experimental Program

2.1. Geometrical Representation of Local Corrosion Morphology

In practical engineering applications, the steel tube corrosion is mostly local corrosion, as shown in Figure 1a. To scientifically quantify and characterize the geometrical dimensions of local corrosion, three fundamental dimensional parameters are defined [29]: axial corrosion length (l), annular corrosion width (ω), and radial corrosion depth (t'), as shown in Figure 1b. These parameters offer the essential quantitative foundation required for later analysis and assessment.

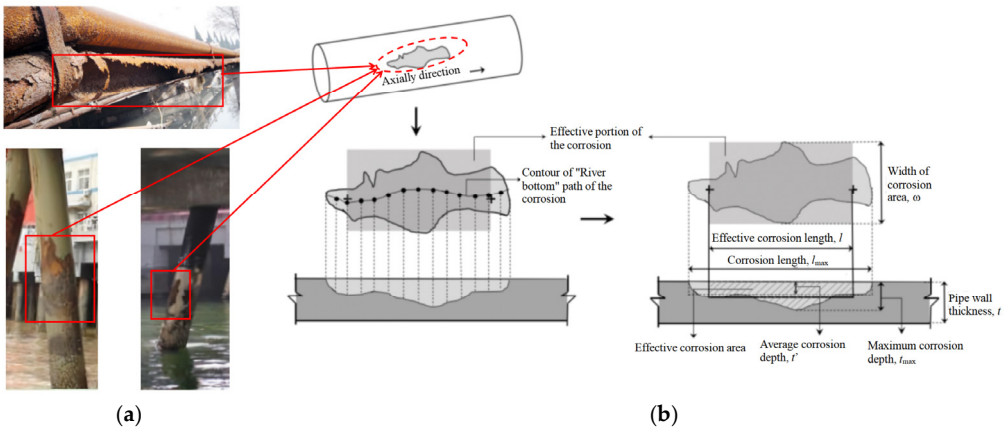

Figure 1. Geometrical characterization of typical local corrosion patterns on steel tube. (**a**) Typical local corrosion patterns. (**b**) Geometrical characterization of typical local corrosion patterns.

2.2. Test Specimen Design and Preparation

A total of 19 CFST axial compression specimens were designed for this study, consisting of specimens with end circumferential-through corrosion, specimens with middle circumferential-through corrosion, and 3 uncorroded control specimens, as illustrated in Figure 2. To simulate the local corrosion defects on the CFST column surfaces, machining techniques, including turning and milling, were initially employed to generate the corrosion defects as expected. Figure 3 presents pictures of the turning in situ and turned steel tube. The corrosion depth was standardized to the average depth of the corrosion area, as depicted in Figure 1b. The detailed parameters of the steel tubes are presented in Table 1. The "CS" in the member number denotes CFST specimen while the letters "N", "T", and "M" indicate uncorroded, end-corroded, and middle-corroded specimens, respectively, as illustrated in Figure 2. The number following these letters represents the wall thickness loss rate, φ_T, of the steel tube. The term "D" refers to the outer diameter of the circular steel tube's cross-section, "t" represents the thickness of the tube wall, and "L" is the calculated length of the member. The axial corrosion proportion, φ_L, is defined as $\varphi_L = l/L$, where

"l" is the length of axial corrosion. The circumferential corrosion proportion, φ_H, is given by $\varphi_H = \omega/H$, with "H" being the perimeter of the steel tube. The wall thickness loss rate, φ_T, is expressed as the ratio of the reduced thickness (t') to the original thickness (t), i.e., $\varphi_T = t'/t$. The volume loss rate of the outer steel tube is denoted by η, determined by the product of the axial, circumferential, and wall thickness loss rates, $\eta = \varphi_L \times \varphi_H \times \varphi_T$. Additionally, "$f_y$" signifies the yield strength of the steel tube, and "f_{cu}" is the compressive strength of the concrete cube.

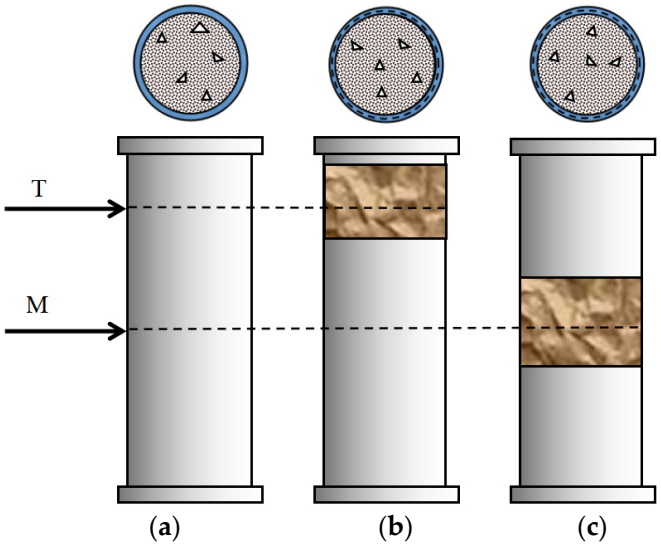

Figure 2. Schematic diagram of corroded CFST. (**a**) CS-N. (**b**) CS-T. (**c**) CS-M.

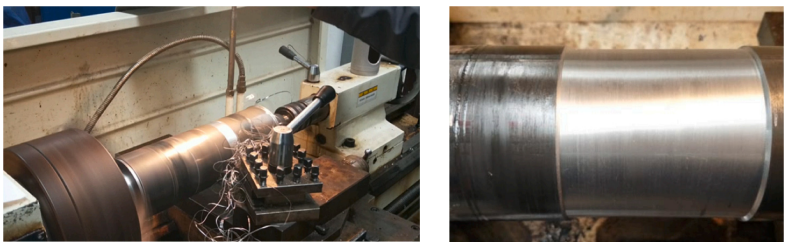

Figure 3. Pictures of the turning in situ and turned steel tube. (**a**) Turning in situ. (**b**) Turned steel tube.

Table 1. Parameters of specimens.

No.	Specimen Number	*D*/mm	*t*/mm	*L*/mm	Corrosion Location	φ_L/%	φ_H/%	φ_T/%	η/%	f_y/MPa	f_{cu}/MPa
1	CS-N0	114	3.64/3.64/3.65	342	——	——	——	——	——	360	55.4
2	CS-T1	114	3.60/3.64	342	upper end	20	100	10	2	360	55.4
3	CS-T3	114	3.64/3.66	342	upper end	20	100	30	6	360	55.4
4	CS-T5	114	3.64/3.67	342	upper end	20	100	50	10	360	55.4
5	CS-T7	114	3.67/3.61	342	upper end	20	100	70	14	360	55.4
6	CS-M1	114	3.69/3.67	342	middle	20	100	10	2	360	55.4
7	CS-M3	114	3.72/3.73	342	middle	20	100	30	6	360	55.4
8	CS-M5	114	3.69/3.70	342	middle	20	100	50	10	360	55.4
9	CS-M7	114	3.70/3.72	342	middle	20	100	70	14	360	55.4

2.3. Axial Compression Test

The axial compression tests were conducted using a NYL-500 hydraulic testing machine manufactured by Changchun Material Testing Machine Factory in Changchun, China. To precisely monitor the strain in various regions of the locally corroded CFST columns, four sets of right-angle strain gauges were symmetrically placed at the center of the corroded area, the center of the non-corroded area, and the boundary of the corroded region.

Additionally, four three lateral linear variable displacement transducers (LVDTs) were installed at the bottom of the loading end. Strain and displacement data were automatically collected by a computerized data acquisition system. The arrangement of the specimen loading device and measurement points are depicted in Figure 4. The test employed a stepwise loading protocol, with each load level in the elastic phase being 1/10 of the design capacity, transitioning to 1/15 of the design capacity in the elastic–plastic phase, and each level being maintained for 2 min. As the load approached the design capacity, a slow and continuous loading rate was applied. If the load decreased to 75% of the theoretical estimated ultimate load capacity or excessive deformation occurred, the specimen was considered damaged, and the test was terminated immediately.

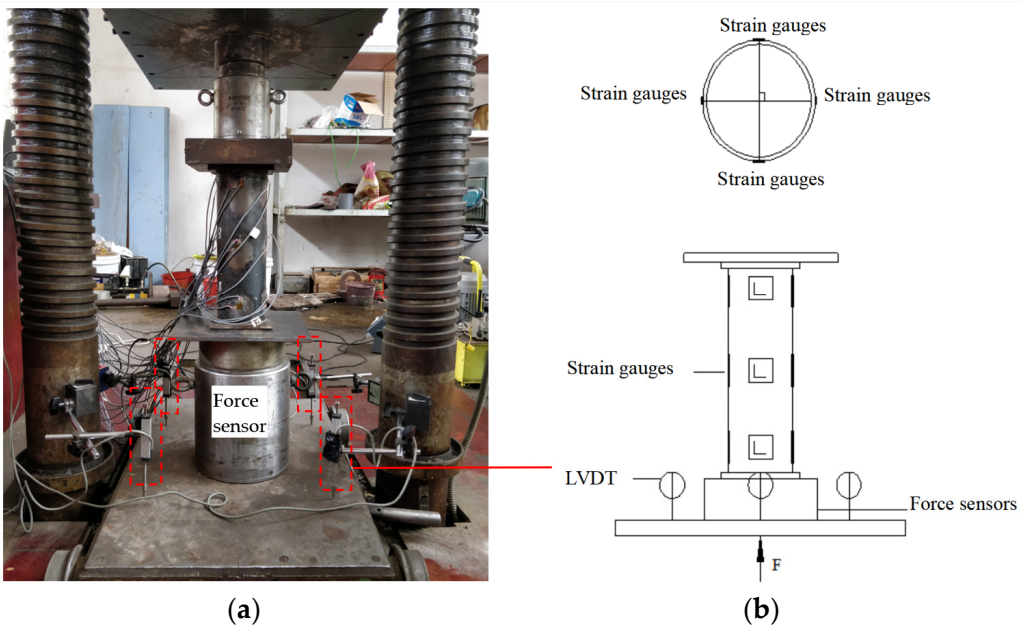

Figure 4. Loading and measuring device. (**a**) Test set-up. (**b**) Layout of measurement points.

3. Test Results and Analysis

3.1. Test Phenomenon

Figure 5 shows the damage patterns of locally corroded CFST columns, all exhibiting a uniform final pattern: local bulging in the corroded areas. When the load reaches approximately 50% of the ultimate load capacity of the specimen, micro-buckling begins in the affected region, with a brief load drop followed by a recovery. As the load further increases, significant local ring buckling appears in the corroded area, leading to the specimen's complete failure and the end of the test. For specimens with a wall thickness corrosion rate below 70%, pronounced drum-type buckling is observed at the ends and middle sections. Conversely, in specimens where the corrosion rate is above 70%, the regions outside the corrosion zone remain almost intact. This difference is attributed to the higher wall thickness corrosion rate, which increases the effective sectional loss of the outer steel tube and weakens its confinement effect to the core concrete. Under axial load, the core concrete in the corroded zone of specimens with a higher wall thickness corrosion rate ($\geq$70%) tends to crush earlier, causing the outer steel tube to bend and the specimen to undergo local bulging deformation and damage, as shown in Figure 5e,j. An increased wall thickness corrosion rate is correlated with earlier local buckling in the corroded region of the outer steel tube and a more significant reduction in the specimen's ultimate bearing capacity. In contrast, specimens with a smaller wall thickness corrosion rate (10%) exhibit final damage morphologies similar to those of uncorroded CFST specimens, as the minor effective cross-sectional loss in the corroded region has a limited impact on the specimens' load bearing.

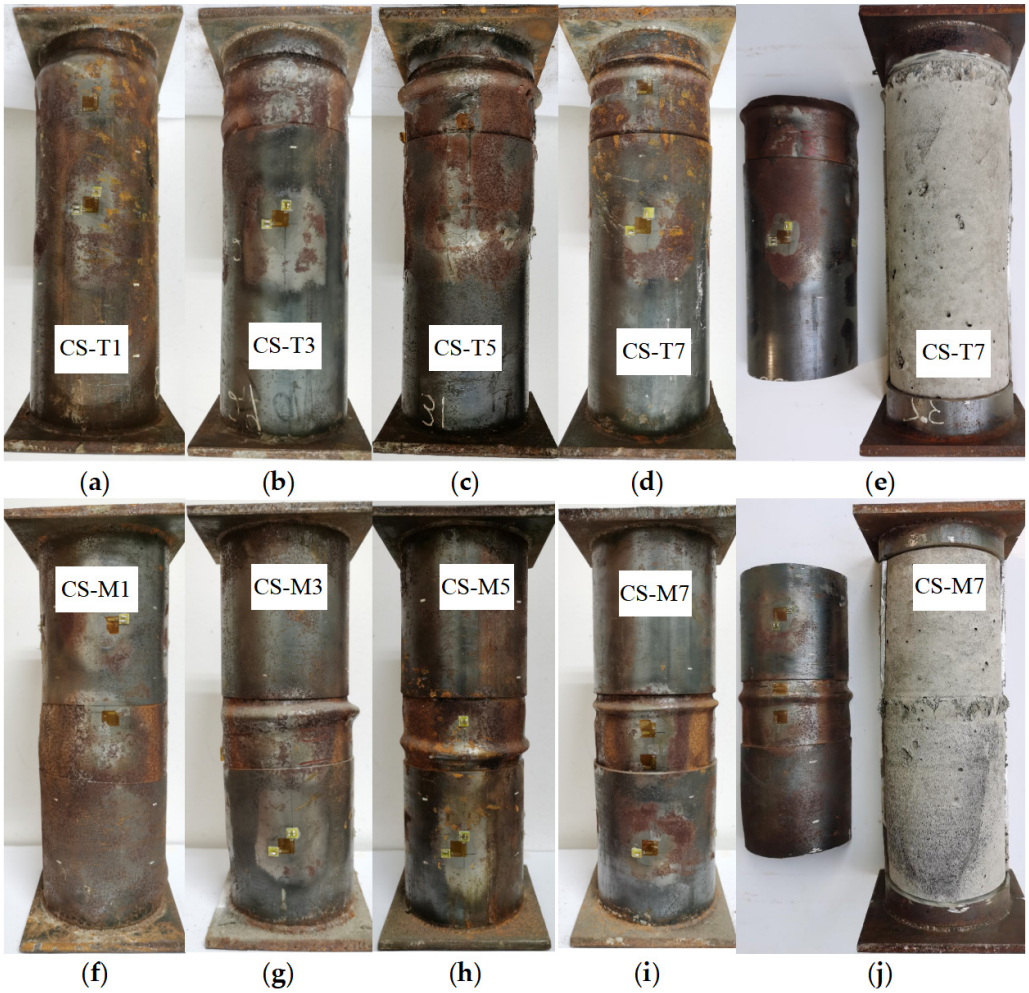

Figure 5. Failure modes of CFST specimens. (**a**) ϕ_T = 10%. (**b**) ϕ_T = 30%. (**c**) ϕ_T = 50%. (**d**) ϕ_T = 70%. (**e**) Typical damage patterns of core concrete. (**f**) ϕ_T = 10%. (**g**) ϕ_T = 30%. (**h**) ϕ_T = 50%. (**i**) ϕ_T = 70%. (**j**) Typical damage patterns of core concrete.

3.2. Load–Displacement Curves of Locally Corroded CFST Columns

Figure 6 presents the axial load–displacement curves for locally corroded CFST columns. When compared to the uncorroded specimen CS-N0 whose load-bearing capacity is 1064 kN, the reduction in load capacity for members with a corrosion rate η of 10% or less ($\varphi_T \leq 50\%$) is minimal, with a decrease of less than 4.1%. At a corrosion rate of 14% (φ_T = 70%), the bearing capacity reduction is more pronounced, with decreases of 7.6% and 4.79% observed for end and middle corroded members, respectively. Upon analyzing the curve's behavior in the Figure, it is evident that when the overall corrosion rate of a specimen is low, the change in mechanical properties due to corrosion is subtle. As the corrosion rate increases, the more pronounced is the reduction in load carrying capacity. Notably, the ductility of specimens with end corrosion is more substantially affected than that of those with middle corrosion. For middle corrosion, although it has an impact on the confinement effect of the core concrete, the confinement of the steel tube in the middle part is relatively weak. Hence, middle corrosion has a relatively smaller influence on the ductility of the specimens. Additionally, middle corrosion has a relatively smaller impact on the bonding performance between the steel tube and concrete. In contrast, end corrosion not only affects the confinement effect at the ends but also may lead to a significant decline in the bonding performance between the steel tube and concrete. This further reduces the ductility of the specimens.

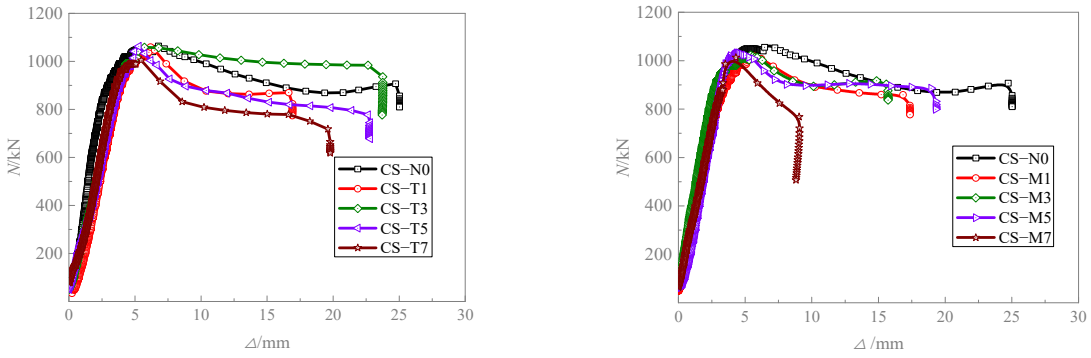

(**a**) (**b**)

Figure 6. Axial load–displacement curve of corroded CFST. (**a**) End circumferentially fully corroded specimens. (**b**)Middle circumferentially fully corroded specimens.

3.3. Stress–Strain Relationship Curve of Local Corrosion Region

Figure 7 presents the stress–strain ($\sigma_{sc} - \varepsilon$) relationship curves for locally corroded CFST columns. The vertical axis represents the nominal compressive stress of the member, calculated as the cross-sectional average compressive stress ($\sigma_{sc} = N/A_{sc}$), where N is the axial compressive load and A_{sc} is the cross-sectional area of the member. The horizontal axis denotes the longitudinal average strain in the local corrosion region. In the initial stage of loading, the load is shared between the core concrete and the steel tube. Stress concentration leads to local bulging of the steel tube in the corroded region, which further evolves into annular buckling, as depicted in Figure 4. Throughout this process, the stress–strain curve transitions from an upward convex to a downward concave shape, indicating a nonlinear change in material behavior. As axial compression increases, the effect of stress redistribution becomes more pronounced, and the core concrete takes on the majority of the increased load. This phenomenon underscores the pivotal role of core concrete in sustaining the overall structural performance, particularly in the instances of local corrosion. In specimens with a substantial tube wall corrosion rate ($\varphi_T > 50\%$), the effective wall thickness of the steel tube in the corrosion region is notably reduced. Despite a decline in bearing capacity, the supportive effect of the core concrete delays the premature local buckling of the thin-walled steel tube in the corroded area, allowing the stress–strain relationship to remain linear until the steel tube yields. When the load exceeds 80% of the ultimate bearing capacity, the specimen transitions into a pronounced elastic–plastic state. During this phase, the steel tube in the corrosion region undergoes waist drum-like deformation.

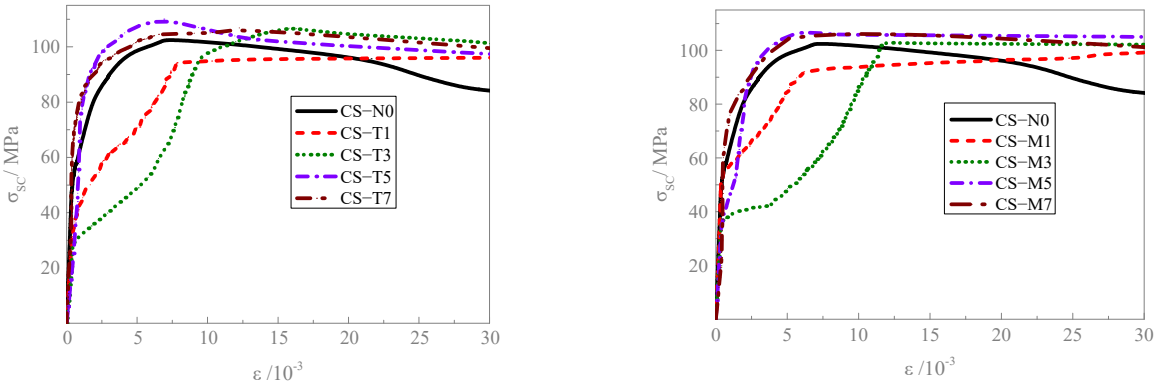

(**a**) (**b**)

Figure 7. Stress–strain curves of corroded CFST. (**a**) End circumferentially fully corroded specimens. (**b**) Middle circumferentially fully corroded specimens.

4. Finite Element Calculation of Locally Corroded CFST

4.1. Establishment of Finite Element Model

The ABAQUS finite element software was used to simulate and analyze the axial load-deformation behavior of CFST columns with local corrosion. For this study, the uniaxial stress–strain relationship model for the core concrete, sourced from the literature [17], is presented with its mathematical formulation in Equation (1)

:

$$y = \begin{cases} 2x - x^2 & x \le 1 \\ 1 + q\left(x^{0.1\xi} - 1\right) & (\xi \ge 1.12)x > 1 \\ x/\left[\beta(x-1)^2 + x\right] & (\xi < 1.12)x > 1 \end{cases} \quad (1)$$

where, $x = \varepsilon/\varepsilon_0$; $y = \sigma/\sigma_0$; $\sigma_0 = \left[1 + \left(-0.054\xi^2 + 0.4\xi\right)(24/f_c)^{0.45}\right]f_c$; $\varepsilon_0 = \left\{\varepsilon_{cc} + [1400 + 800(f_c/24 - 1)]\xi^{0.2}\right\} \cdot (\mu\varepsilon)$; $\varepsilon_{cc} = 1300 + 12.5f_c$; $q = \xi^{0.745}/(2 + \xi)$; $\beta = \left(2.36 \times 10^{-3}\right)^{0.25+(\xi-0.5)^7} \cdot (f_c)^2 \times 3.51 \times 10^{-4}$; ξ reflects the combined action between the steel tube and the core concrete, $\xi = \alpha f_y / f_{ck}$, α is the steel content, f_{ck} is the standard value of concrete compressive strength; f_c is the concrete cylinder compressive strength.

In the ABAQUS software, the steel material is defined using the "Plastic" model, which represents its plastic properties with a five-stage secondary plastic flow model. For uncorroded members, the model specifies the steel tube's wall thickness as the initial thickness (t). In the case of corroded members, the wall thickness of the outer steel tube within the corroded area is adjusted to reflect the remaining effective wall thickness, accounting for the loss of material due to corrosion [17]. For other material properties, refer to the literature [28].

The computational mechanical model of the CFST column is constructed as a three-dimensional entity and uses C3D8R solid elements. The mesh density is increased in the corroded zone of the steel tube to achieve higher precision in the numerical simulation results. The interface contact between the steel tube and concrete is face-to-face. Along the normal direction of the contact surface, hard contact is assumed. While along the tangent direction, bond–slip contact is assumed, and the penalty function of the Coulomb friction model with a friction coefficient of 0.6 is used. The contact surface between the endplate and concrete is assumed to be "hard contact" in the normal direction and negligible in the tangential direction. The endplate and the outer steel tube are regarded as tied constraints. The loading process and boundary conditions are shown in Figure 8. Displacement loading is applied at one end, and the other endplate is fixed. At the fixed end, three-directional linear displacement constraints (U1, U2, U3) and two out-of-plane rotation constraints (UR1, UR3) are imposed, and the in-plane rotation constraint (UR2) is not considered. For the loading end, the z-direction linear displacement (U3) is free, and the other boundary constraints are the same as those of the fixed end. In the numerical analysis, the elastic modulus and Poisson's ratio of the endplate are set as 1012 MPa and 0.0001, respectively, to make it appear rigid.

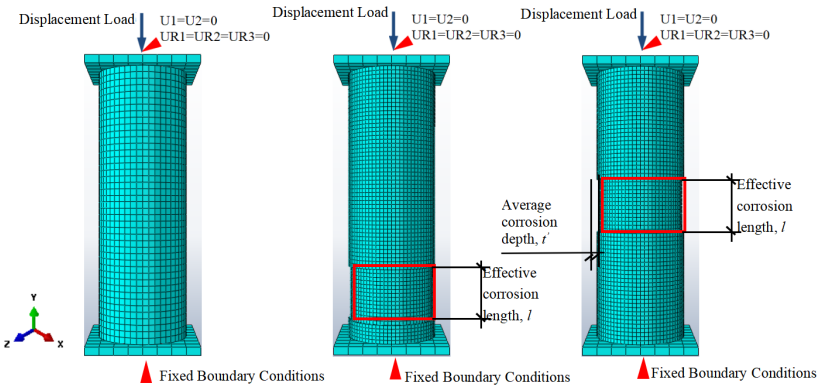

Figure 8. Numerical model of CFST columns.

4.2. Finite Element Model Validation

Figure 9 presents the load–displacement relationship curves of corroded CFST columns. The experimental data are in good correlation with the finite element simulation results, indicating that the peak load values from the tests are close to the simulated values.

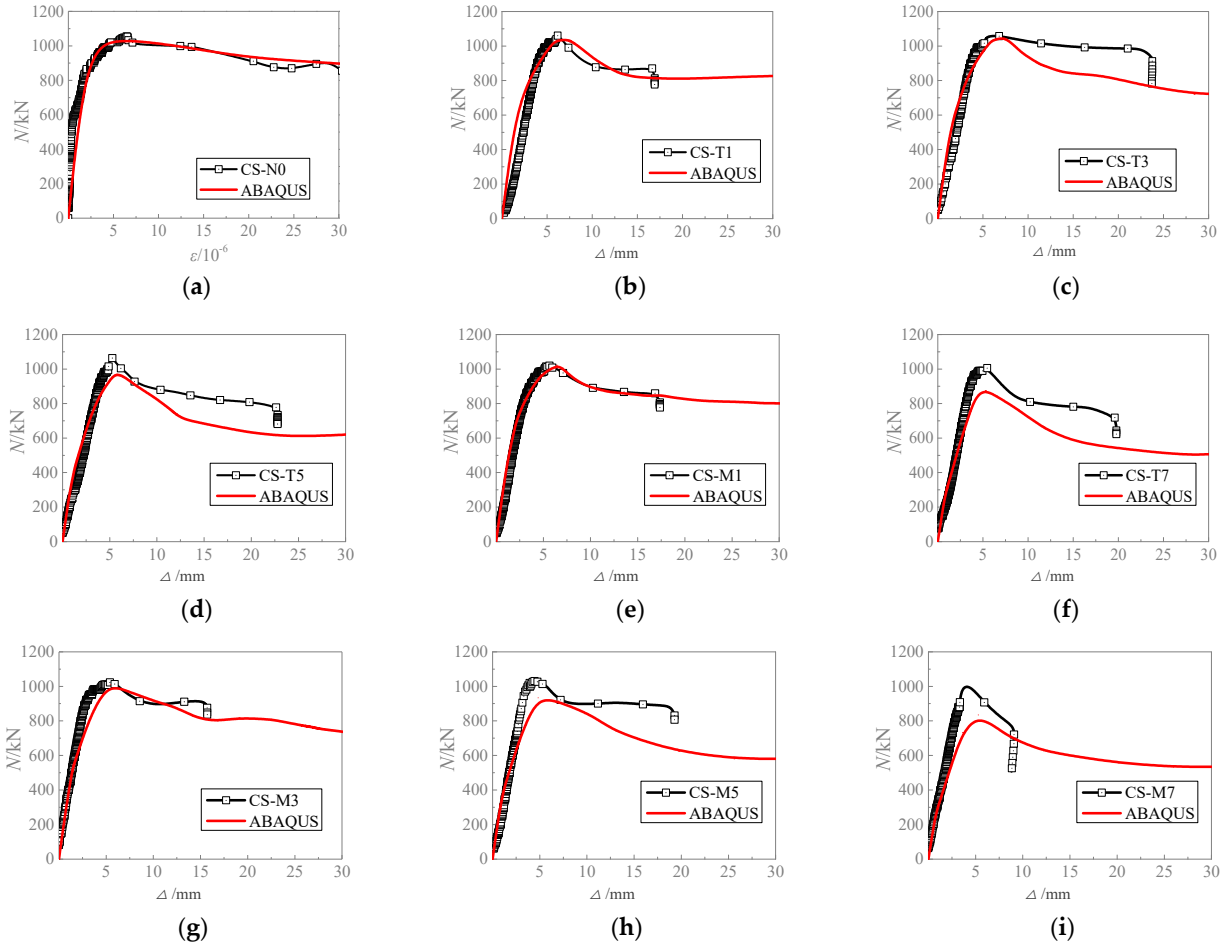

Figure 9. Comparison of test results and simulation results of corroded CFST columns. (**a**) CS-N0. (**b**) CS-T1. (**c**) CS-T3. (**d**) CS-T5. (**e**) CS-T7. (**f**) CS-M1. (**g**) CS-M3. (**h**) CS-M5. (**i**) CS-M7.

4.3. Comparison of Damage Patterns

Figure 10 presents a comparative analysis between finite element simulations and experimental damage patterns of corroded CFST columns. Experimental observations indicate that at approximately 50% of the ultimate load, the end region of the specimen initiates a minor bulge, which progresses to a pronounced annular bulge deformation as the load increases, finally leading to specimen failure. The finite element simulation's maximum stress contour plot reveals stress concentration in the end corrosion region, with the simulated damage morphology closely matching the experimental outcomes. Figure 10b illustrates the scenario where the local corrosion region is positioned in the middle of the specimen. The final damage morphology of both the test and numerical simulation is the ring buckling of the local corrosion region. The computational results of the FEA model are in good agreement with the test results.

Upon comparing the test and finite element calculation results for locally corroded CFST columns, it is evident that the finite element model developed in this study effectively simulates the stress response and failure modes of the corroded columns. This validation confirms the effectiveness of the numerical method employed in predicting the mechanical behavior of structures subjected to local corrosion.

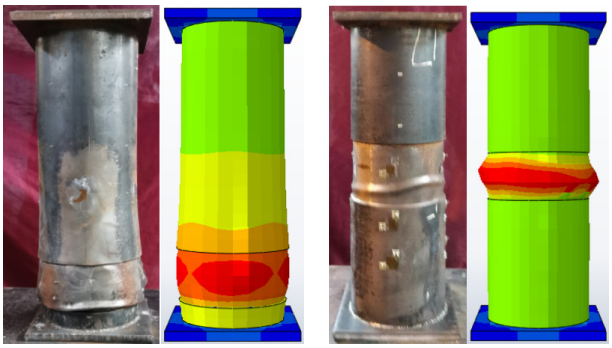

(**a**) (**b**)

Figure 10. Comparisons of failure modes. (**a**) CS-T7. (**b**) CS-M7.

5. Parametric Analysis

This section provides a comprehensive analysis of the load–deformation relationship of locally corroded CFST columns, using a finite element model to explore the impact of local corrosion on axial compressive load capacity. The analysis considers variations in the three-dimensional characteristics of the corroded region and its geometric spatial location. To ensure the universality of the conclusions, dimensionless parameters are employed to characterize the dimensions of the local corrosion region. The circumferential corrosion ratio, φ_H, is defined as the ratio of the corroded width ω to the perimeter H, equivalent to the ratio of the corroded angle θ to a full circle (360°). φ_H adopts values of 0.17, 0.33, 0.50, 0.67, 0.83, and 1.00, corresponding to θ angles of 60°, 120°, 180°, 240°, 300°, and 360°, respectively. The wall-thickness corrosion ratio, φ_T, is calculated as the ratio of the corrosion depth t' to the initial wall thickness t of the steel tube. φ_T encompasses values of 0.1, 0.2, 0.4, 0.6, and 0.8. Assuming the initial wall thickness t is 4 mm, the corresponding corrosion depth t' are 0.4 mm, 0.8 mm, 1.6 mm, 2.4 mm, and 3.2 mm, respectively. The axial corrosion ratio, φ_L, is defined as the ratio of the corroded length l to the total column height L, with values of 0.2, 0.4, 0.6, 0.8, and 1.0. Given the test CFST column height L is 342 mm, the corresponding corroded lengths l are 68.4 mm, 136.8 mm, 205.2 mm, 273.6 mm, and 342 mm, respectively.

5.1. Effect of Local Corrosion Location

This section investigates the impact of local corrosion on the axial compressive mechanical properties of the steel tube surface at varying locations by developing a numerical model of a CFST column with local corrosion, as depicted in Figure 11. The corrosion regions were deliberately placed at specific locations along the column's length: the top end (T), upper middle (U), middle (M), lower middle (D), and bottom end (B), to assess their influence on structural performance.

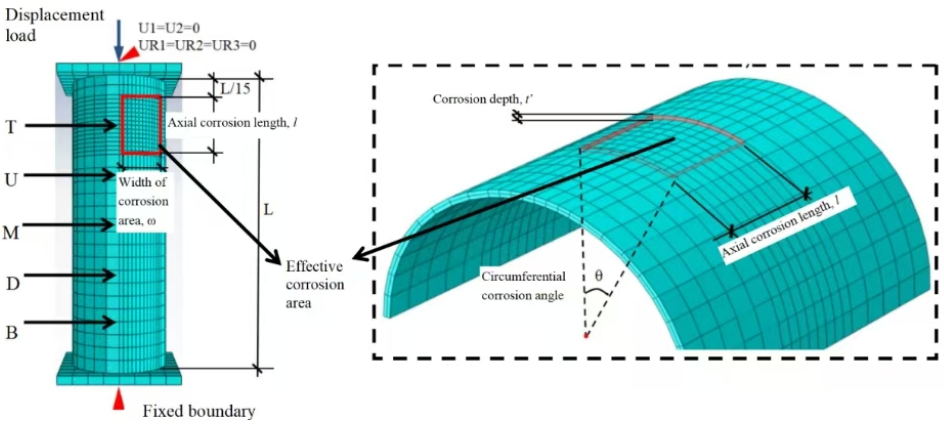

Figure 11. Schematic diagram of numerical model CFST columns with local corrosion.

Figure 12 presents a diagram depicting the change in axial compressive load-bearing capacity for CFST columns with local corrosion at different locations. The Figure reveals that the load bearing capacity diminishes as the wall thickness corrosion rate increases. At low corrosion rates ($\eta < 4\%$), the load-bearing capacity is minimally affected by the location of corrosion, with the maximum reduction being no more than 5%. Typically, the most detrimental location for local corrosion is in the middle-region of the CFST column length (M). With the increase in the corrosion rate, the location that has the most significant impact shifts gradually; generally, corrosion in the middle-region of the specimen (U, M, D) exerts a more pronounced effect on the load-carrying capacity than that at the ends (T, B). This susceptibility is likely due to the mid-section region being more prone to stress concentration and local buckling under axial compression, resulting in a diminished load-carrying capacity. Nevertheless, the variation range of the load-carrying capacity of each CFST column with the same corrosion rate at different positions is still within 10%.

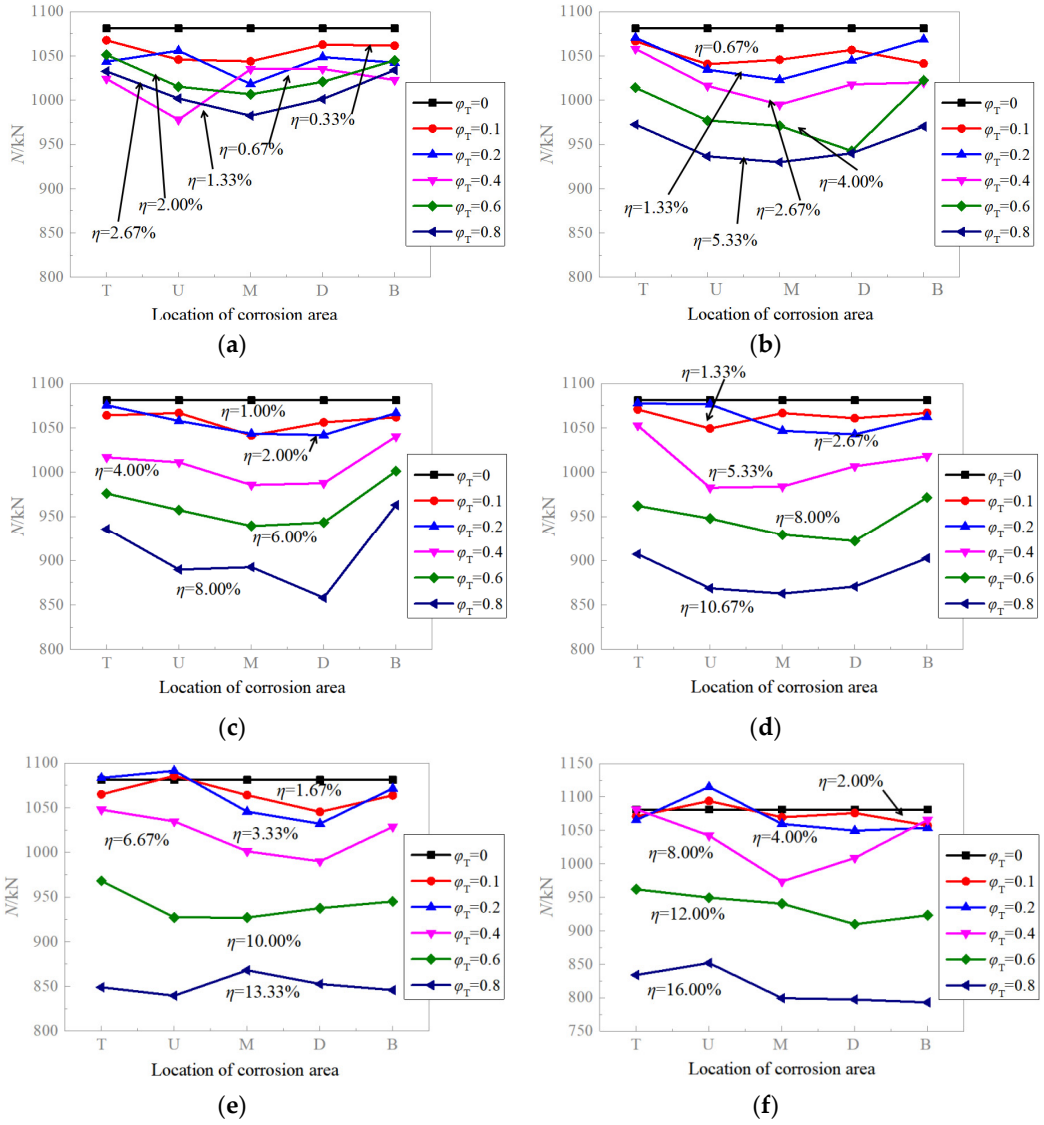

Figure 12. Change pattern of bearing capacity of CFST columns with different local corrosion locations. (**a**) $\phi_H = 0.17$, $\phi_L = 0.2$ ($\theta = 60°$, $l = L/5$). (**b**) $\phi_H = 0.33$, $\phi_L = 0.2$ ($\theta = 120°$, $l = L/5$). (**c**) $\phi_H = 0.50$, $\phi_L = 0.2$ ($\theta = 180°$, $l = L/5$). (**d**) $\phi_H = 0.67$, $\phi_L = 0.2$ ($\theta = 240°$, $l = L/5$). (**e**) $\phi_H = 0.83$, $\phi_L = 0.2$ ($\theta = 300°$, $l = L/5$) (**f**) $\phi_H = 1.00$, $\phi_L = 0.2$ ($\theta = 360°$, $l = L/5$).

Figure 13 illustrates the stress distribution, represented by stress cloud, for the CFST columns under axial compression, with variations attributed to different local corrosion

locations. The local corrosion regions are characterized by a wall thickness corrosion rate (φ_T) of 0.8, an annular corrosion ratio (φ_H) of 0.33, and an axial corrosion ratio (φ_L) of 0.2. Figure 12 illustrates that uncorroded CFST columns typically manifest central drum-type buckling damage when subjected to axial compression. However, introducing local corrosion defects to the column surface leads to abrupt alterations in the cross-section. The presence of local corrosion defects on the surface of a steel tube can lead to abrupt changes in the cross-sectional area. These variations can weaken the confining effect of the outer steel tube on the core concrete, simultaneously disrupting the path of axial stress transfer within the structure. This results in uneven stress distribution around the corroded area, with local stress concentrations occurring at the edges of the corrosion area. As a consequence, the steel tube in the corroded region reaches the yielding stage at lower loads, which adversely affects the specimen's load-carrying capacity. Local corrosion significantly modifies the mechanical response of the CFST specimen. It not only diminishes the load-carrying capacity but also induces a shift in the failure mode. Instead of occurring in the central region, buckling damage at the time of specimen failure is shifted to the cross-section containing the local corrosion area.

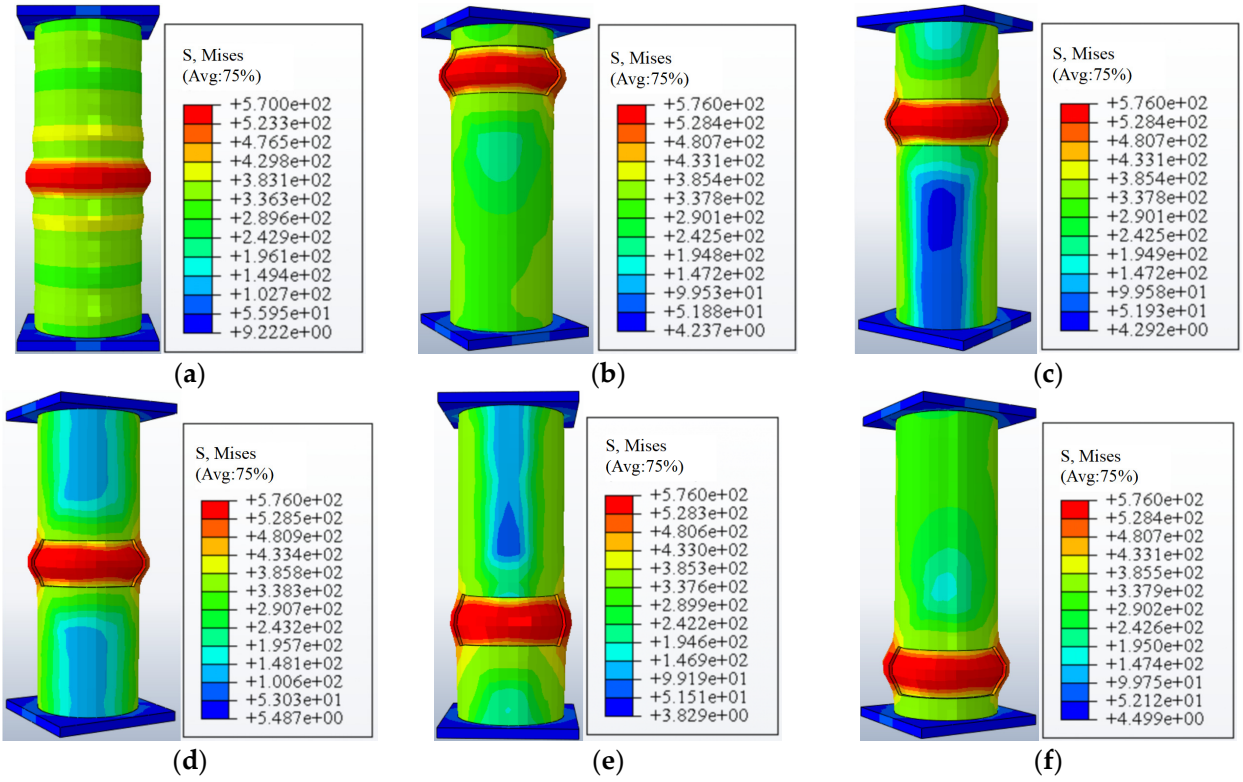

Figure 13. Stress distribution diagram of CFST columns with different local corrosion locations. (**a**) uncorroded. (**b**) Top end. (**c**) Upper middle. (**d**) Middle. (**e**) Lower middle. (**f**) Bottom end.

5.2. Effect of Circumferential Corrosion Ratio

Figure 14 presents the variation curves of the load-bearing capacity of CFST columns across different circumferential corrosion ratios. With the increase of the circumferential corrosion ratio, the load-bearing capacity shows a distinct downward trend. Notably, at a low wall thickness corrosion rate, as shown in Figure 14a,b, the influence of the circumferential corrosion ratios on the load-carrying capacity is minimal, and the maximum reduction is less than or equal to 10%. In addition, when the axial corrosion ratio exceeds 0.2, the load-bearing capacity curves tend to converge. This indicates that under conditions of higher corrosion rates, the circumferential corrosion ratio has a more substantial impact on the specimen-bearing capacity than the axial corrosion ratio.

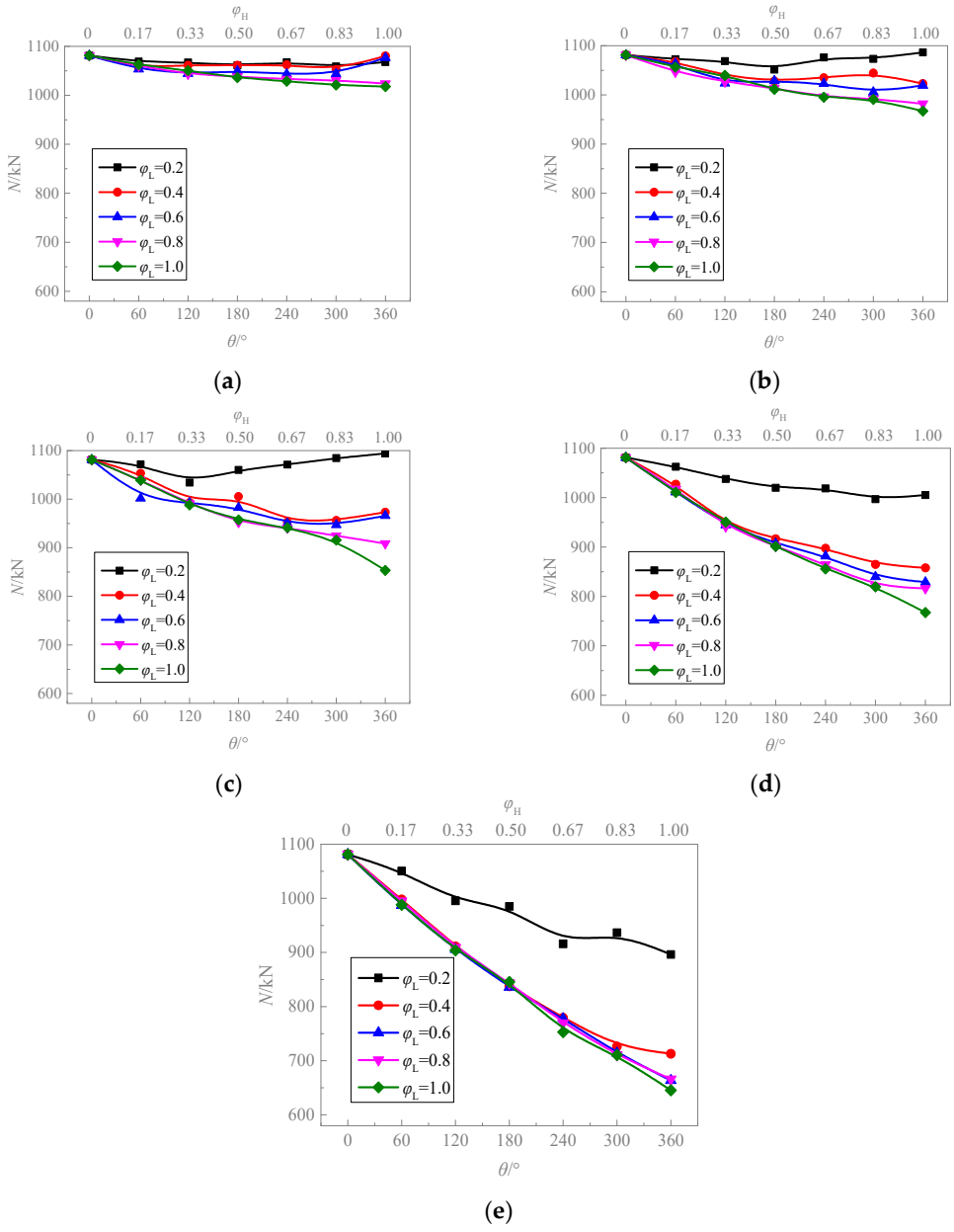

Figure 14. Change curve of the bearing capacity of CFST columns with $\varphi_{H.}$ (**a**) φ_T = 0.1. (**b**) φ_T = 0.2. (**c**) φ_T = 0.4. (**d**) φ_T = 0.6. (**e**) φ_T = 0.8.

Figure 15 presents the stress cloud distributions calculated by finite element analysis for the CFST columns with different circumferential corrosion ratios. The local corrosion regions are defined by a wall thickness corrosion rate of 0.2 and an axial corrosion ratio of 0.2. The Figure clearly shows that local corrosion leads to stress concentration within the CFST column under axial compression. The stress concentration in uncorroded columns is typically located at the mid-height of the specimen. However, the presence of local corrosion shifts the region of maximum stress to the center of the corroded area. As the circumferential corrosion angle increases, the location of stress concentration moves from the center of the corrosion defect towards the inner edge of the corrosion area, eventually forming a stress cloud ring at the boundary of the corrosion zone. The failure mode of the specimen transitions from the typical uniform circular bulging of uncorroded specimens to a shear-type failure, resulting in a reduction in the ultimate load-bearing capacity. When the circumferential corrosion angle reaches 360°, pronounced stress cloud rings emerge at

the top and the fixed end of the corroded region, ultimately leading to annular buckling damage in the local corrosion area and drum-like damage at the column ends.

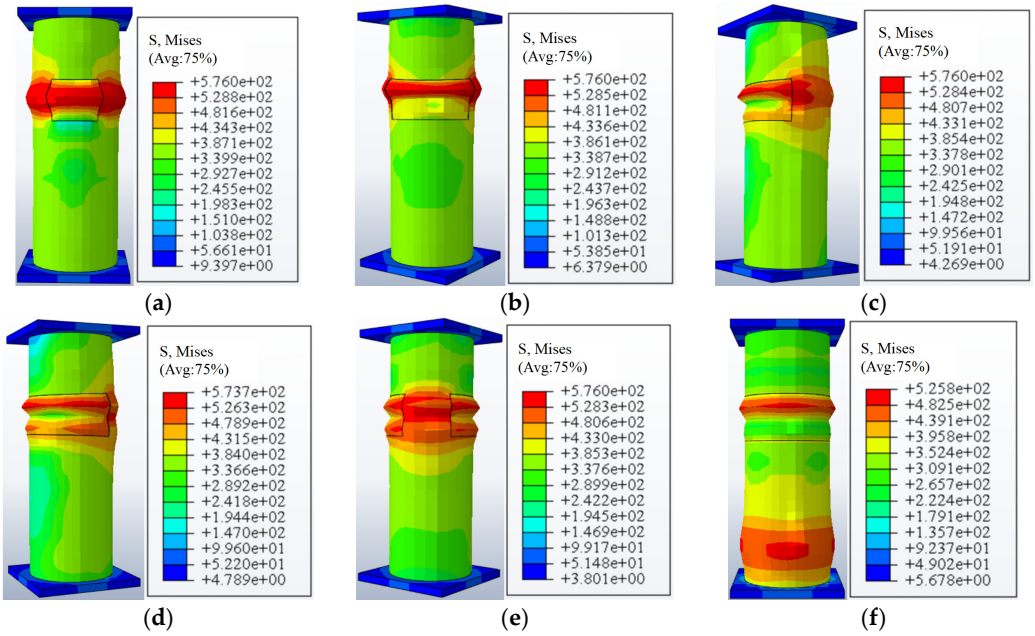

Figure 15. Stress distribution diagram of CFST columns with different circumferential corrosion ratios. (**a**) φ_H = 0.17. (**b**) φ_H = 0.33. (**c**) φ_H = 0.67. (**d**) φ_H = 0.50. (**e**) φ_H = 0.83. (**f**) φ_H = 1.00.

5.3. Effect of Axial Corrosion Ratio

Figure 16 presents the curves of variations in the load-bearing capacity for the CFST columns with varying axial corrosion ratios. Observing the Figure, it is obvious that the overall trend of load-bearing capacity declines with an increasing axial corrosion ratio. At low wall thickness corrosion rates ($\varphi_T \leq 0.2$), as depicted in Figure 16a,b, the impact of axial corrosion ratios on the load-carrying capacity is minimal, with the maximum reduction not exceeding 10%. With higher wall thickness corrosion rates, the bearing capacity shows a greater reduction when the axial corrosion ratios increase, suggesting that the expansion of the local corrosion area significantly affects the structural integrity. However, when the axial corrosion ratio exceeds 0.2, the bearing capacity curve levels off. This implies that once a certain threshold is exceeded, the further increase in the axial corrosion ratio has a diminishing impact on the load-bearing capacity.

Figure 17 presents the stress cloud distributions calculated by finite element analysis for the CFST columns with different axial corrosion ratios. The local corrosion regions are defined by a wall thickness corrosion rate of 0.4 and a circumferential corrosion ratio of 0.83. During the loading process, a ring-shaped stress concentration cloud initially forms at the edge of the boundary in the locally corroded region. Concurrently, strip-like stress concentration clouds emerge in the middle of the non-corroded region. This phenomenon is attributed to the stress redistribution that occurs as axial compression is transmitted through the uncorroded areas. As the axial corrosion ratio increases, these stress concentration clouds migrate toward the center of the corroded region, eventually forming a continuous stress concentration cloud ring. This development culminates in drum-type buckling damage within the locally corroded area of the specimen. Overall, the increase in the axial corrosion ratio mainly affects the location of the stress concentration cloud ring, while having a relatively minor impact on its distribution pattern. This indicates that while the axial expansion of the corroded region alters the position of the most severe stress concentration, the fundamental pattern of stress distribution remains consistent.

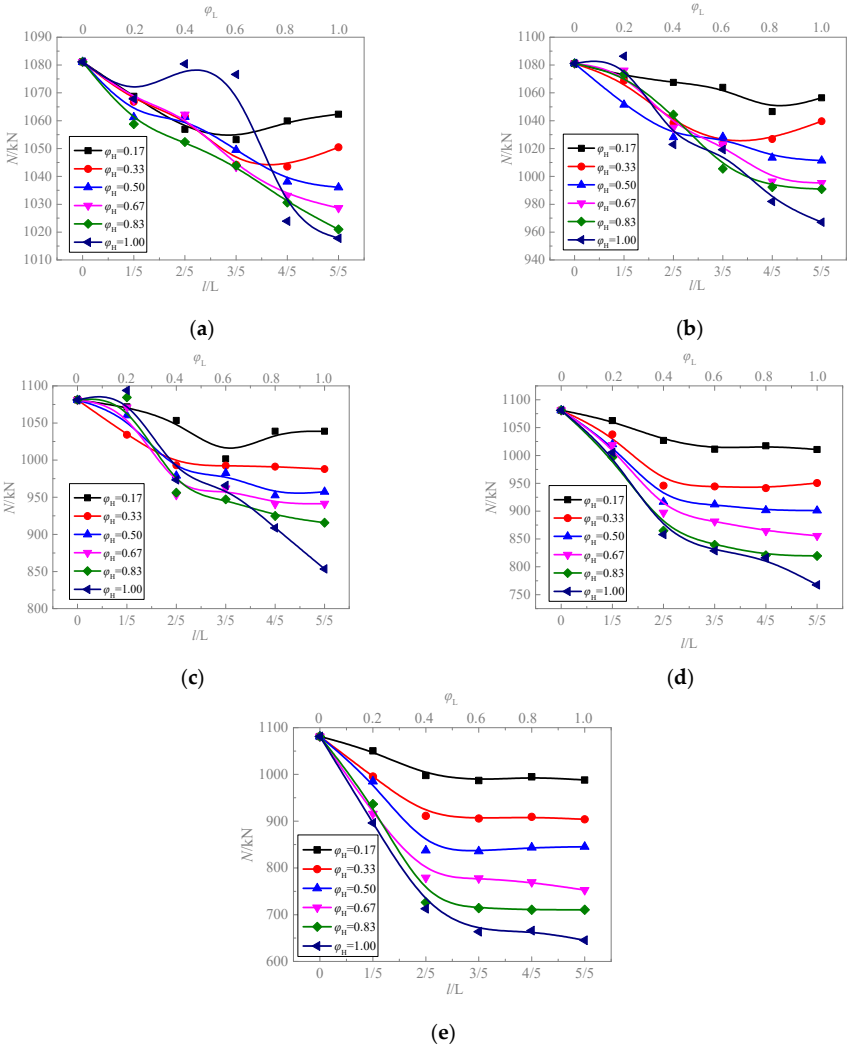

Figure 16. Change curve of the bearing capacity of CFST columns with φ_L. (**a**) φ_T = 0.1. (**b**) φ_T = 0.2. (**c**) φ_T = 0.4. (**d**) φ_T = 0.6. (**e**) φ_T = 0.8.

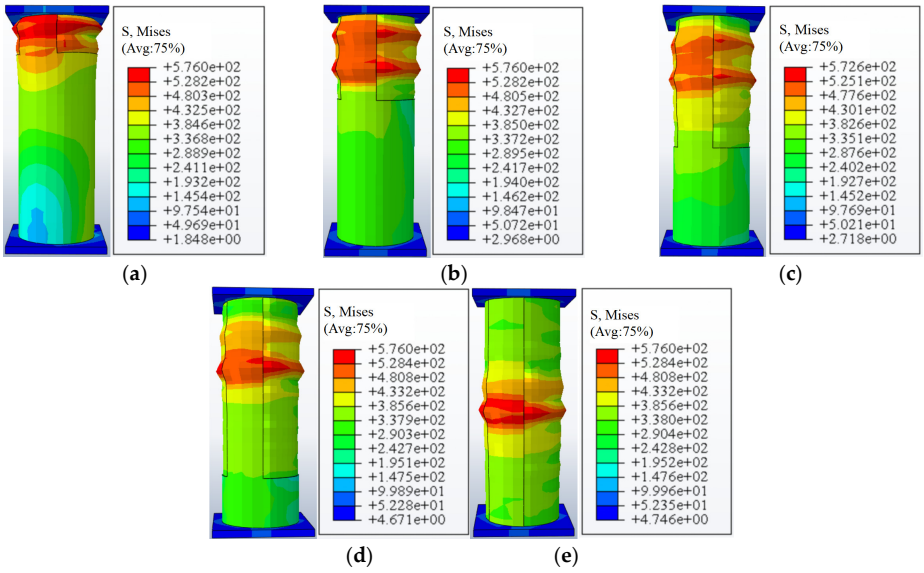

Figure 17. Stress distribution diagram of CFST with different axial corrosion ratios. (**a**) φ_L = 0.2. (**b**) φ_L = 0.4. (**c**) φ_L = 0.6. (**d**) φ_L = 0.8. (**e**) φ_L = 1.00.

5.4. Effect of Wall Thickness Corrosion Rate

Figure 18 displays the curves of variation in the load-carrying capacity for the CFST columns across different wall thickness corrosion rates. At an axial corrosion ratio of 0.2, as shown in Figure 18a, the load-bearing capacity generally exhibits a downward trend in correlation with the increasing wall thickness corrosion rate. Notably, until the wall thickness corrosion rate (φ_T) reaches 0.52, the changes between the load-bearing capacity curves for different circumferential corrosion ratios lack a clear pattern. This inconsistency may be attributed to the interplay of stress concentration and corrosion rate during the loading process, particularly at low corrosion rates. Beyond $\varphi_T = 0.52$, the load-carrying capacity experiences a significant decline with the most substantial reduction reaching 19%. This suggests that at low corrosion rates, the wall thickness corrosion rate is a pivotal factor influencing the load-carrying capacity. As the axial corrosion ratio increases, as depicted in Figure 17b, the load-carrying capacity decreases further. When φ_T reaches 0.2, the reduction in capacity is already 5%. An additional increase in φ_T results in a pronounced gradient among the bearing capacity change curves, indicating that a higher degree of corrosion has a more pronounced impact on the bearing capacity. Figure 18c,d illustrates the substantial decrease in bearing capacity as the three-dimensional dimensions of the local corrosion region expand. In summary, at higher corrosion rates, the three-dimensional extent of the corroded region predominantly affects the load-carrying capacity. The wall thickness corrosion rate is identified as the most influential factor, followed by the circumferential corrosion ratio, with the axial corrosion ratio being the least significant.

Figure 19 presents the stress cloud distributions, as calculated by finite element analysis, for CFST columns with different wall thickness corrosion rates. The local corrosion regions are characterized by a circumferential corrosion ratio of 0.17 and an axial corrosion ratio of 0.83. Observing the figure, it is evident that as the corrosion depth increases, the stress concentration within the corrosion region intensifies, and the area of maximum stress concentration expands. At a low wall thickness corrosion rate ($\varphi_T = 0.1$), even with the presence of a stress concentration cloud in the corrosion region, the maximum stress in the steel tube has not reached the yield stress at the time of failure. The overall stress distribution across the specimen remains relatively uniform, and the damage morphology resembles that of an uncorroded specimen, exhibiting a girdle-shaped damage pattern. However, as the corrosion depth increases, the corrosion region begins to exhibit noticeable local buckling damage. This indicates that the impact of local corrosion on the stress distribution and damage morphology of CFST columns becomes increasingly significant with an increasing wall thickness corrosion rate.

In conclusion, the influence of local corrosion on the axial stress performance of CFST columns is primarily observed through stress concentration during loading and a reduction in axial bearing capacity. At low corrosion rates, the change in bearing capacity for locally corroded steel tube concrete columns is not pronounced. Specifically, when the planar dimensions of the locally corroded area are small ($\varphi_L < 0.2$, $\varphi_H \leq 0.67$), the axial bearing capacity is predominantly influenced by stress concentration during loading and the corrosion rate. As the corrosion rate increases, particularly for larger planar dimensions of the locally corroded area ($\varphi_L \geq 0.2$, $\varphi_H > 0.67$), the corrosion rate emerges as a primary factor affecting the axial bearing capacity. Once the planar size of the corroded area surpasses a certain threshold, the impact of the annular effective section loss rate on the load-carrying capacity becomes substantial, whereas the additional influence of the axial corrosion ratio on the load-carrying capacity is minimal.

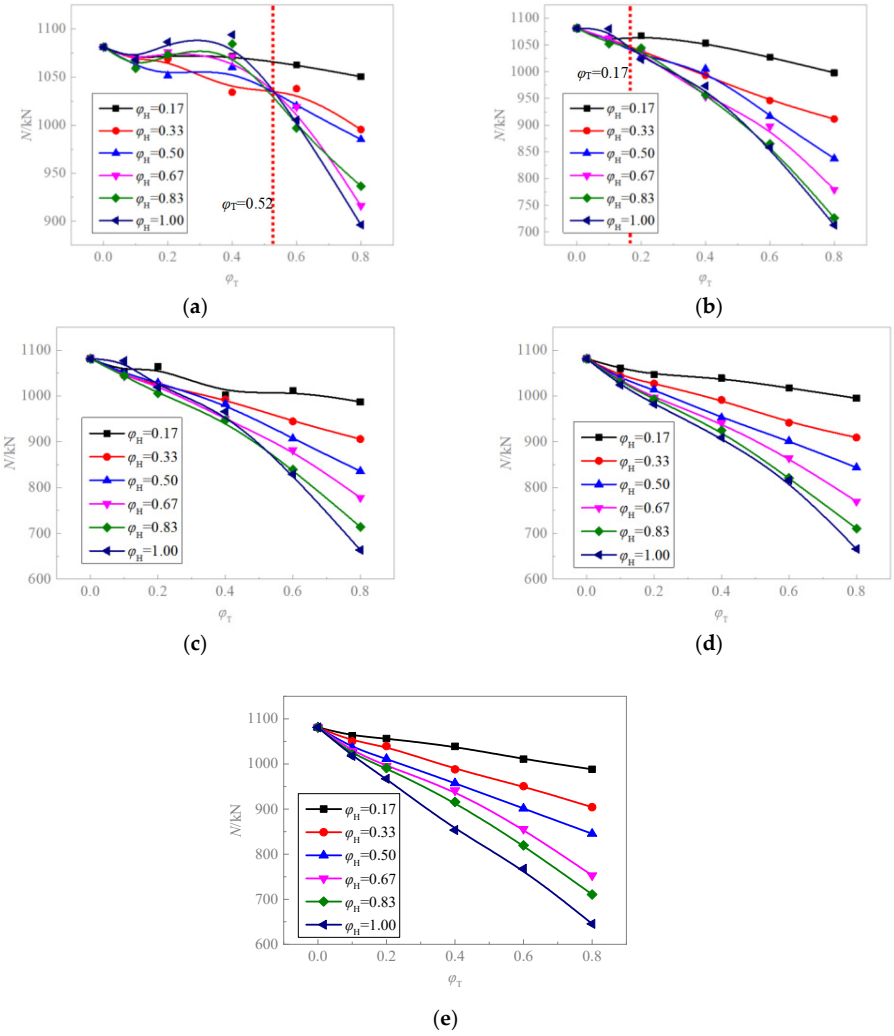

Figure 18. Change curve of the bearing capacity of CFST columns with φ_T. (**a**) ϕ_L = 0.2 (l = L/5). (**b**) ϕ_L = 0.4 (l = 2L/5). (**c**) ϕ_L = 0.6 (l = 3L/5). (**d**) ϕ_L = 0.8 (l = 4L/5). (**e**) ϕ_L = 1.0 (l = L).

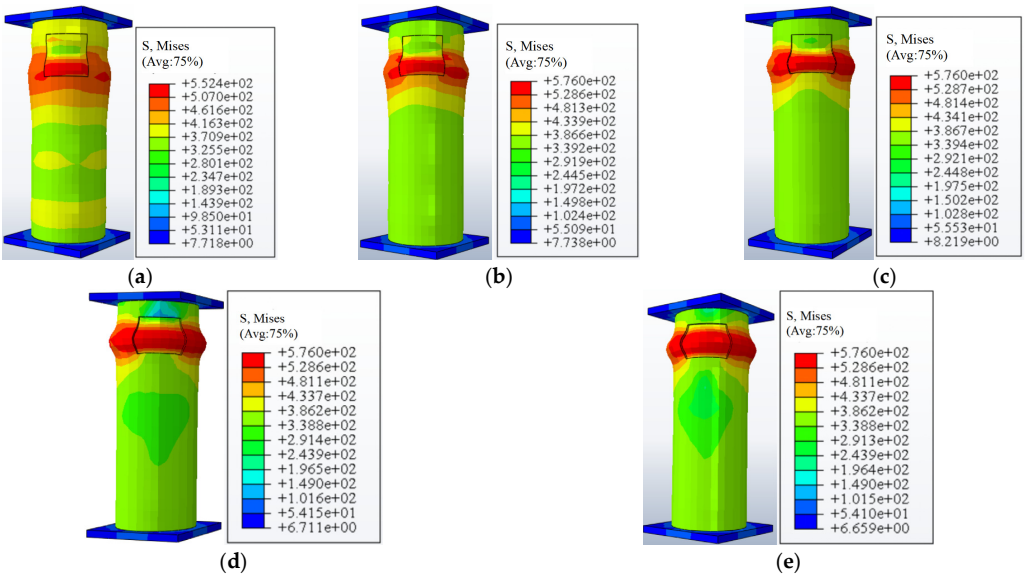

Figure 19. Stress distribution diagram of CFST columns with different wall thickness corrosion rates. (**a**) φ_T = 0.1. (**b**) φ_T = 0.2. (**c**) φ_T = 0.4. (**d**) φ_T = 0.6. (**e**) φ_T = 0.8.

6. Practical Model for Axial Compressive Load Capacity Calculation

6.1. Practical Model for Calculating CFST Axial Compressive Load Capacity Affected by Local Corrosion

The GB 50936-2014 Technical Code for Steel Tube Concrete Structures [30] provides a formula for calculating the axial compressive bearing capacity of CFST as follows:

$$N_{u0} = A_{sc} \cdot f_{sc} \tag{2}$$

where: N_{u0} is the design value of axial compressive load capacity of the short CFST column; A_{sc} is the cross-sectional area of CFST member; f_{sc} is the strength index of CFST in axial compression, given by the expression $f_{sc} = (1.212 + B\xi + C\xi^2) f_c$, where ξ reflects the combined action between the steel tube and the core concrete; f_c is the design value of the compressive strength of concrete. B and C are factors representing the influence of the cross-sectional shape on the confinement effect coefficient, calculated as $B = 0.176 f_{ye}/213 + 0.974$ and $C = -0.104 f_{ck}/14.4 + 0.031$, respectively. f_{ye} is the effective yield strength of the corroded steel tube [17], determined by $f_{ye} = (1 - 1.007\beta_w) f_y$.

The impact of local corrosion on the bearing capacity of CFST is multifaceted. Firstly, it results in the loss of the effective cross-sectional area of the outer steel tube, which weakens the hoop effect that the steel tube exerts on the core concrete. Secondly, the abrupt change in the cross-sectional area due to local corrosion can lead to stress concentration within the specimen, thereby affecting its bearing capacity. Thirdly, the reduction in the effective cross-sectional area causes a shift in the center of gravity of the specimen, making the actual loading pattern resemble that of a small eccentric load.

To quantitatively characterize the impact of local corrosion on the bearing capacity of CFST, this paper introduces a corrosion influence coefficient, denoted as K_{corr}, which is defined as follows:

$$K_{corr} = 1 - \alpha_{cs} \tag{3}$$

Here, α_{cs} represents the degradation rate of the bearing capacity of CFST, accounting for the effects of local corrosion, calculated as $\alpha_{cs} = (N_{u0} - N_{ue})/N_{u0}$; where N_{ue} is the axial compressive load-bearing capacity of the corroded CFST column; and N_{u0} is that of the uncorroded column.

As previously mentioned, the geometrical spatial location of the corroded area on a CFST column under axial compression has a negligible effect on the load-bearing capacity, with deviations not exceeding 10%. To facilitate practical engineering applications, this paper proposes a formula, derived from test results and finite element analysis, to statistically assess the impact of local corrosion on the bearing capacity degradation of steel tube concrete columns. This formula disregards the location of the corrosion region and focuses solely on the three-dimensional dimensions of the corrosion region's impact on the axial compressive capacity of steel tube concrete. The formula is as follows:

$$\alpha_{cs} = \phi_T \phi_L \phi_H (C - \phi_L) + k\phi_L \phi_H (D + \phi_L - \lambda\phi_H) \tag{4}$$

By substituting Equation (4) into the previously defined Equations (2) and (3), one can obtain the bearing capacity calculation formula for a locally corroded CFST column:

$$N_{ue} = K_{cs} N_{u0} = N_{u0}[1 - \phi_T \phi_L \phi_H (C - \phi_L) - k\phi_L \phi_H (D + \phi_L - \lambda\phi_H)] \tag{5}$$

where C, D, k, and λ are fitting coefficients. Utilizing the experimental data and finite element simulation results from this paper, the values for these parameters are "1.45, 1.6, 0.0277, 2.4", respectively.

6.2. Comparison of Theoretical Predictions with Test Values for Load Capacity

Figure 20 presents a comparison between the calculated results derived from the proposed formula (Equation (5)) and the numerical test results, including a 95% confidence interval. The Figure reveals that 93.2% of the data points fall within this confidence interval,

signifying that the formula is highly reliable in capturing the trend of the numerical test results. The calculated values closely align with the finite element simulation results, with a ratio ranging from 0.89 to 1.07.

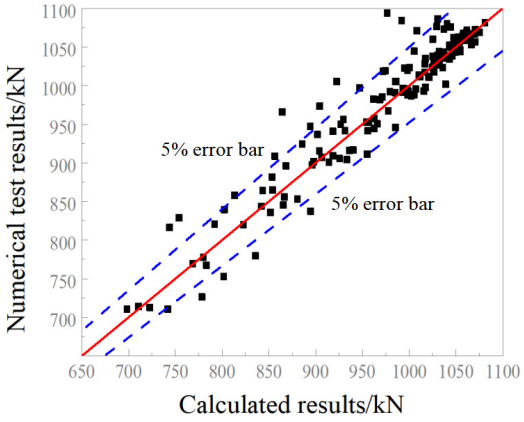

Figure 20. Comparison chart of simplified formula calculation results and numerical test results.

Table 2 details the comparative analysis of the test values for the specimens, the finite element calculated values, and the load-carrying capacities predicted by the formulae. Here, N_{cs} denotes the measured load-carrying capacity of the members, N_{csf} represents the load-carrying capacity from finite element simulations, and N_{ue} is the load-carrying capacity determined by the formulae proposed in this study. According to Table 2, the average ratio of N_{cs} to N_{csf} is 1.04, with a variance of 0.005, indicating that the finite element simulation results closely match the test values, thereby demonstrating high simulation accuracy. Similarly, the average ratio of N_{cs} to N_{ue} is 1.03, with a variance of 0.003, which suggests that the bearing capacity calculation formula proposed in this paper also predicts the load-carrying capacity of the members with a high accuracy. The data in the table confirm that both the finite element simulation and the formulae presented in this paper are effective in calculating the bearing capacity of locally corroded steel tube concrete columns.

Table 2. Comparison of simplified formula calculation results and test results.

Specimen Number	φ_T/%	η/%	N_{cs}/kN	N_{csf}/kN	N_{ue}/kN	N_{cs}/N_{csf}	N_{cs}/N_{ue}
CS-N0	——	——	1064	1055.49	1073.09	1.008	0.992
CS-T1	10	2	1023	1038.20	1037.67	0.985	0.986
CS-T3	30	6	1048	1039.91	1000.2	1.008	1.048
CS-T5	50	10	1063	971.17	955.117	1.094	1.113
CS-T7	70	14	983	875.36	908.603	1.123	1.082
CS-M1	10	2	1020	1021.11	1048.14	0.999	0.973
CS-M3	30	6	1023	1010.67	1010.24	1.012	1.013
CS-M5	50	10	1032	933.641	959.219	1.105	1.077
CS-M7	70	14	1013	834.865	915.11	1.213	1.107
CS-A0 [17]	——	——	883	895	877	0.987	1.007
CS-A1 [17]	9.4	9.4	834	844	839	0.988	0.994
CS-A2 [17]	20.4	20.4	760	769	794	0.988	0.957

7. Conclusions

This paper presents an in-depth investigation into the effects of local corrosion, considering both its location and three-dimensional dimensions on the axial compressive load-bearing capacity of CFST columns. Through a synergistic approach of experimental testing and ABAQUS finite element simulations, the corresponding load capacity calculation formulae have been developed. The conclusions drawn from this study are as follows:

(1) Local corrosion on the surface of steel tubes leads to a sudden change in cross-section, causing stress concentration and consequently reducing the axial compressive bearing

capacity and ductility of CFST columns. The impact is more pronounced when the corrosion is located in the middle section of the specimen compared to the ends. Nevertheless, when local corrosion defects of the same size occur at different axial positions of the CFST column, the variation range of its bearing capacity is within 10%.

(2) The increase in corrosion rate is positively correlated with the downward trend of bearing capacity. Under the same corrosion rate, the change in the three-dimensional size of the local corrosion area will significantly affect the mechanical properties of the CFST columns.

(3) When the planar dimensions of the locally corroded area are small ($\varphi_L < 0.2$, $\varphi_H \leq 0.67$), the variation in axial compressive load capacity of CFST columns is primarily influenced by stress concentration during loading and the corrosion rate itself; the wall thickness corrosion rate, circumferential corrosion ratio, and axial corrosion ratio have a minor impact on the load-carrying capacity, with no clear pattern. As the corrosion rate increases, particularly for larger planar dimensions of the locally corroded area ($\varphi_L \geq 0.2$, $\varphi_H > 0.67$), the three-dimensional dimensions of the corroded area become the predominant factors affecting load-carrying capacity. Among these, the wall thickness corrosion rate has the most significant effect, followed by the circumferential and axial corrosion rates. Additionally, once the axial corrosion ratio reaches a certain threshold ($\varphi_L > 0.2$), its further impact on the load-carrying capacity is minimal.

(4) The paper has proposed a formula for calculating the axial compressive load capacity of locally corroded CFST columns. This formula demonstrates high accuracy and reliability when validated against test results and finite element simulations.

(5) This formula does not consider various complex corrosion morphologies that may occur in practical engineering. Although it can preliminarily evaluate the impact of local corrosion on the axial compressive bearing capacity of CFST columns when detailed corrosion information is lacking, its ability to assess structural behavior under complex corrosion morphologies is limited. Future research still needs to develop a more comprehensive model to accurately consider complex corrosion characteristics and their impact on structural integrity and provide stronger support for practical engineering applications.

Author Contributions: Methodology, H.H.; Validation, K.X.; Data curation, Q.W. and R.Z.; Writing—original draft, W.F.; Conceptualization, Writing—review & editing, M.C. All authors have read and agreed to the published version of the manuscript.

Funding: This research was funded by the National Natural Science Foundation of China (Grant Nos. 52468022 and 52278180) and the Natural Science Foundation of Jiangxi Province of China (Grant No. 20232BAB214071).

Data Availability Statement: The original contributions presented in the study are included in the article, further inquiries can be directed to the corresponding author.

Acknowledgments: We greatly appreciate the anonymous reviewers for offering us good comments.

Conflicts of Interest: The authors declare no conflict of interest.

References

1. Dewanbabee, H.; Das, S. Structural behavior of corroded steels pipes subject to axial compression and internal pressure: Experimental study. *J. Struct. Eng.* **2012**, *139*, 57–65. [CrossRef]
2. Li, G.; Hou, C.; Shen, L.M. Life-cycle analysis of FRP-strengthened offshore CFST columns suffering from steel corrosion. *Compos. Struct.* **2021**, *277*, 114607. [CrossRef]
3. Thai, S.; Thai, H.T.; Uy, B.; Ngo, T. Concrete-filled steel tubular columns: Test database, design and calibration. *J. Constr. Steel Res.* **2019**, *157*, 161–181. [CrossRef]
4. Han, L.H.; Hou, C.; Wang, Q.L. Square concrete filled steel tubular (cfst) members under loading and chloride corrosion: Experiments. *J. Constr. Steel Res.* **2012**, *71*, 11–25. [CrossRef]
5. Hou, C.; Han, L.H.; Zhao, X.L. Full-range analysis on square CFST stub columns and beams under loading and chloride corrosion. *Thin-Walled Struct.* **2013**, *68*, 50–64. [CrossRef]

6. Hou, C.C.; Han, L.H.; Wang, Q.L.; Hou, C. Flexural behavior of circular concrete filled steel tubes (CFST) under sustained load and chloride corrosion. *Thin-Walled Struct.* **2016**, *107*, 182–196. [CrossRef]
7. Han, L.H.; Hua, Y.X.; Hou, C.; Wang, Q.-L. Circular concrete-filled steel tubes subjected to coupled tension and chloride corrosion. *J. Struct. Eng.* **2017**, *143*, 04017134. [CrossRef]
8. Hua, Y.X.; Han, L.H.; Wang, Q.L.; Hou, C. Behavior of square CFST beam-columns under combined sustained load and corrosion: Experiments. *Thin-Walled Struct.* **2019**, *136*, 353–366. [CrossRef]
9. Wang, Q.L.; Li, Q.L.; Qu, S.E. Experimental study on corrosion resistance property of circular concrete filled steel tubular beam under long-term loading. *J. Build. Struct.* **2015**, *36* (Suppl. 2), 50. (In Chinese)
10. Wang, Q.L.; Feng, L.M.; Qu, S.E. Experimental study on axially compressed circular concrete-filled steel tubular stub columns under long-term coupling effects of loading and chloride corrosion. *China Civ. Eng. J.* **2015**, *48* (Suppl. 1), 48–52. (In Chinese)
11. Ma, D.Y.; Ma, S.; Xu, L.Y. Reliability analysis of axial compressive strength of concrete-filled steel tube (CFST) under coupled corrosion and load effects. *Buildings* **2024**, *14*, 3205. [CrossRef]
12. Gao, S.; Guo, L.H.; Zhang, S.M.; Peng, Z. Performance degradation of circular thin-walled CFST stub columns in high-latitude offshore region. *Thin-Walled Struct.* **2020**, *154*, 106906. [CrossRef]
13. Zhang, F.J.; Xia, J.W.; Li, G.; Guo, Z.; Chang, H.F.; Wang, K.J. Degradation of axial ultimate load bearing capacity of circular thin-walled concrete-filled steel tubular stub columns after corrosion. *Materials* **2020**, *13*, 795. [CrossRef] [PubMed]
14. Zhang, T.; Lyu, X.T.; Liu, H.Q.; Zhang, L.Q.; Wang, J.F.; Gao, S. Axial performance degradation of squared CFST stubs in severe cold and acid rain area. *Constr. Build. Mater.* **2020**, *262*, 120612. [CrossRef]
15. Yuan, F.; Chen, M.C.; Huang, H. Square CFST columns under cyclic load and acid rain attack: Experiments. *Steel Compos. Struct.* **2019**, *30*, 171–183.
16. Yuan, F.; Chen, M.C.; Huang, H.; Xie, L.; Wang, C. Circular concrete filled steel tubular (CFST) columns under cyclic load and acid rain attack: Test simulation. *Thin-Walled Struct.* **2018**, *122*, 90–101. [CrossRef]
17. Chen, M.C.; Fang, W.; Huang, H.; Wang, C.; Liu, J.J. Axial compressive behavior of recycled concrete filled corroded circular steel tubular columns. *J. Build. Struct.* **2019**, *40*, 138–146. (In Chinese) [CrossRef]
18. Melchersr, E. Progress in developing realistic corrosion models. *Struct. Infrastruct. Eng.* **2018**, *14*, 843–853. [CrossRef]
19. Mohammed, A.A.; Manalo, A.C.; Ferdous, W.; Zhuge, Y.; Vijay, P.V.; Alkinani, A.Q.; Fam, A. State-of-the-art of prefabricated FRP composite jackets for structural repair. *Eng. Sci. Technol. Int. J.* **2020**, *23*, 1244–1258. [CrossRef]
20. Huang, C.; Chen, T.; Wang, X. Compressive characteristics of damaged circular hollow section (CHS) steel columns repaired by CFRP or grout jacketing. *Thin-Walled Struct.* **2017**, *119*, 635–645. [CrossRef]
21. Guo, L.H.; Huang, H.J.; Jia, C.; Romanov, K. Axial behavior of square CFST with local corrosion simulated by artificial notch. *J. Constr. Steel Res.* **2020**, *174*, 106314. [CrossRef]
22. Huang, H.J.; Guo, L.H.; Qu, B.; Jia, C.; Elchalakani, M. Tests of circular concrete-filled steel tubular stub columns with artificial notches representing local corrosions. *Eng. Struct.* **2021**, *242*, 112598. [CrossRef]
23. Li, G.; Hou, C.; Shen, L.M.; Yao, G.H. Performance and strength calculations of CFST columns with local pitting corrosion damage. *J. Constr. Steel Res.* **2022**, *188*, 107011. [CrossRef]
24. Li, G.; Hou, C.; Shen, L.M. Combined compression-bending performance and design of CFST with localised pitting corrosion. *J. Constr. Steel Res.* **2022**, *192*, 107247. [CrossRef]
25. Zhao, Z.W.; Gao, T.; Jian, X.Y.; Mo, S.J.; Liu, B.B. Eccentric compression capacity of circular CFST columns under random pitting corrosion. *Ocean. Eng.* **2023**, *288*, 115975. [CrossRef]
26. Li, J.W.; Jia, C.; Gao, S.; Guo, L.H. Experimental and numerical study on axial compression behavior of slender CFST columns with localized pitting corrosion damage. *Constr. Build. Mater.* **2024**, *414*, 134858. [CrossRef]
27. Jia, C.; Li, J.W.; Guo, L.H.; Zhong, L. Behavior of stub SCFST columns with localized pitting corrosion damage. *Eng. Fail. Anal.* **2024**, *156*, 107824. [CrossRef]
28. Luo, S.C.; Chen, M.C.; Huang, H.; Xv, K.; Fang, W.; Zhang, R. Eccentric compression test and ultimate load strength analysis of circular CFST long column with local corrosion. *Structures* **2023**, *56*, 104937. [CrossRef]
29. Siraj, T.; Zhou, W.X. Evaluation of statistics of metal-loss corrosion defect profile to facilitate reliability analysis of corroded pipelines. *Int. J. Press. Vessel. Pip.* **2018**, *166*, 107–115. [CrossRef]
30. *GB 50936-2014*; Technical Code for Steel Tube Concrete Structures. China Architecture & Building Press: Beijing, China, 2014.